HANSER

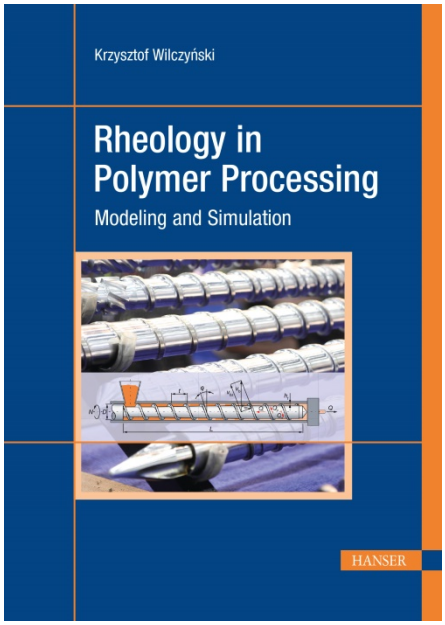

Sample Pages

Rheology in Polymer Processing

Krzysztof Wilczyński

ISBN (Book): 978-1-56990-660-6
ISBN (E-Book): 978-1-56990-661-3

For further information and order see

www.hanserpublications.com (in the Americas)

www.hanser-fachbuch.de (outside the Americas)

Preface

This book is designed to provide a polymer rheology background for polymer processing to both engineering students and practicing engineers. It is written on an intermediate, sometimes advanced level, required to enable the reader to understand the complex rheological behavior of polymers and its far reaching consequences in polymer processing.

There are many excellent books on polymer rheology as well as polymer processing and process modeling. However, this book is comprehensive with content that allows the reader to understand how the engineering CAD/CAE software for process modeling works, and also how this is developed, which makes its use more conscious and effective. This book is written to bridge the gap between a science and an engineering practice. It begins with fundamentals of rheology and ends on using and applications of CAD/CAE software.

The first chapter covers the basics of rheology, i.e. the basics of continuum mechanics, including the concepts of stress, rate of strain, constitutive equations, as well as the concepts of viscosity and viscoelasticity. Tensor notation is used here for a better understanding of these concepts. This notation allows us to generalize simple one-dimensional problems to three-dimensional problems, as well as to consider simple problems as special cases of complex problems.

The second chapter covers the basics of rheometry, which is a science concerning the measurement of rheological properties of polymers, and thus on the measurements of stress and strain. These are made using rheometers. Good rheological material data are the basis for the correct modeling of polymer processing. Understanding the issues of measuring the rheological properties of polymers, including their limitations, is important for the informed use of CAD/CAE systems.

The third chapter describes the basic processing techniques, and three steps of processing are distinguished: pre-processing or compounding in which chemically pure polymers are prepared for processing, such as mixing and pelletizing, polymer processing in which products are formed, e.g. extrusion, injection molding, thermoforming, and post-processing or complementary processing, i.e. finishing treatment of manufactured products.

The fourth chapter covers the modeling of polymer processing, which is applied to better understand the manufacturing processes. Analytical solutions for some simple flow problems are presented, which can be used to solve a lot of engineer-

ing problems. However, most of the polymer processing models are represented by sets of non-linear partial differential equations and/or integral equations, which do not have analytical solutions. These problems can be solved using methods of numerical analysis.

The fifth chapter covers the modeling of polymer extrusion, which is the most important technology in the polymer processing industry since more than half of all polymers are extruded. Moreover, extrusion is fundamental for compounding, i. e. mixing, pelletizing, filling, and reinforcing. The first and fundamentals models of polymer processing were developed for single screw extrusion, and these early concepts are still highly important in modeling of polymer processing.

The sixth chapter describes the software for computer modeling of polymer processing. The selected flow problems are solved using ANSYS Polyflow for CFD modeling, Autodesk Moldflow for injection molding, and MULTI-SCREW for extrusion. These programs enable the modeling of most problems in polymer processing.

In this book, the references are limited to books, with the exception of the sixth chapter, which contains also the author's papers. The historically first and fundamental books on rheology and fluid mechanics are referenced, i. e. those by Reiner (1949), Eirich et al. (1956), and Bird et al. (1960), then chronologically, e. g. by Tanner (1985), Bird et al. (1987), White (1990), Macosko (1994), Carreau et al. (1997), until the current books, e. g. by Vlachopoulos (2016). The historically first and fundamental books on polymer processing and process modeling are also referenced, i. e. by Bernhardt et al. (1959), Schenkel (1959), and McKelvey (1962), then chronologically, e. g. by Tucker (1987), Hensen et al. (1989), White and Potente (2002), Tadmor and Gogos (2006), Rauwendaal (2013), until the current books e. g. by Agassant et al. (2017).

The author would like to acknowldge the invaluable help of his colleagues at the Polymer Processing Department at the Warsaw University of Technology during the preparation of this manuscript. In particular I would like to thank Dr. Andrzej Nastaj for co-authorship of the chapter on modeling of extrusion and for development of figures throughout the book, Dr. Adrian Lewandowski for co-authorship of the chapter on CFD modeling, Dr. Krzysztof J. Wilczyński for co-authorship of the chapter on modeling of injection molding, and my PhD student MSc Kamila Buziak for preparing the manuscript. I thank Dr. Mark Smith of Hanser Publishers for his co-operation during the production of this book.

I would like to dedicate this book to the memory of Professor James Lindsay White of the University of Akron, who passed away a little over 10 years ago (1938–2009), and who creatively inspired me to research work during my Fulbright scholarship at The University of Akron, and later. Professor John Vlachopoulos of McMaster University and Professor Avraam Isayev of The University of Akron are cordially thanked for their support throughout this project.

Summer 2020 *Krzysztof Wilczyński*

Warsaw, Poland

Contents

1 Rheology

1.1 Fundamentals of Continuum Mechanics

1.1.1 Stress

If external forces act on a material medium (body), they induce forces in that medium that affect each cross-section of the body. The surface density of these forces is called the **stress.**

The forces acting on a material medium can be characterized as body forces or surface forces. **Body forces** act on every mass element of the medium and are proportional to its total mass. They do not affect the geometrical form of the body. Examples of body forces are gravity forces, inertia forces, or electromagnetic forces. These forces affect any body; however, a physical contact with the surroundings in which these forces occur is not necessary. On the other hand, in the case of **surface forces,** contact with the surroundings is necessary. These forces do not depend on the mass of the medium, but on the size of the surface they operate on. They affect the geometrical form of the body, causing it to deform. Examples of surface forces are pressure forces or viscosity forces.

At the state of equilibrium, the mass and surface forces balance each other. But in motion, the algebraic sum of these forces is proportional to the product of mass and acceleration of the body, according to the second principle of Newton's dynamics.

In order to define the concept of stress, we make an analysis of forces acting on the body, as shown in Figure 1.1. In this body, a surface element ΔS is selected, on which an elementary force $\Delta \underset{\sim}{\boldsymbol{F}}$ acts at a point P. The position of an element ΔS is defined by the vector $\underset{\sim}{\boldsymbol{r}}$, and its direction by the normal unit vector $\underset{\sim}{\boldsymbol{n}}$. The unit force acting on this elementary surface is defined as the stress vector $\underset{\sim}{\boldsymbol{f}}$.

$$\underset{\sim}{\boldsymbol{f}} = \lim_{\Delta S \to 0} \left(\frac{\Delta \underset{\sim}{\boldsymbol{F}}}{\Delta S} \right) \tag{1.1}$$

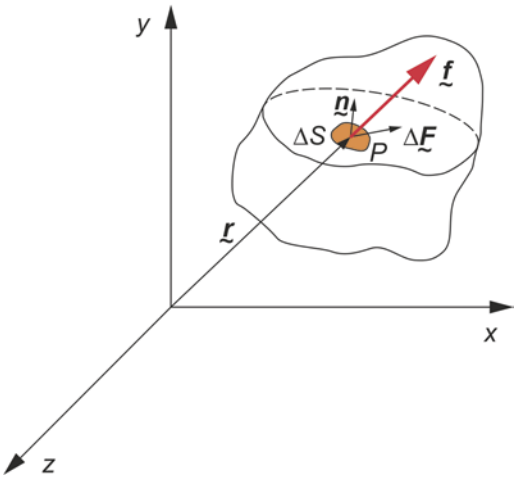

Figure 1.1
The stress vector $\underset{\sim}{f}$

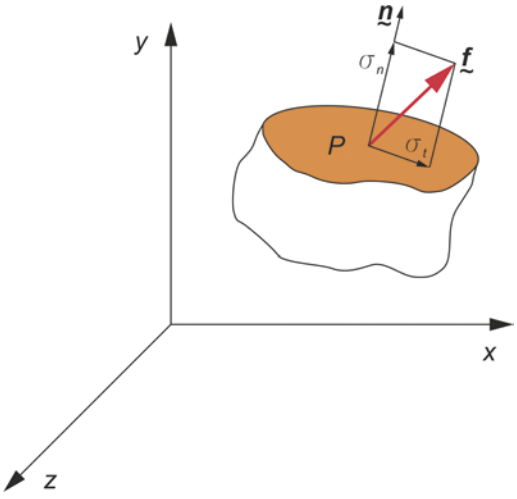

Figure 1.2
Components of the stress vector $\underset{\sim}{f}$:
σ_n – normal stress, σ_t – shear stress

The component of the stress vector $\underset{\sim}{f}$ normal to the surface dS is defined as the **normal stress** σ_n, while the component parallel to that surface is the **tangential (shear) stress** σ_t (Figure 1.2).

The stress vector $\underset{\sim}{f}$ cannot characterize the state of stress at a given point in the body because it depends on the orientation of the surface element dS, i. e., on the vector $\underset{\sim}{n}$. The state of stress at a point P is characterized by the relation of vectors $\underset{\sim}{f}$ and $\underset{\sim}{n}$, that is, by the **stress tensor** $\underset{\sim}{\sigma}(\underset{\sim}{r})$. It is defined by the product

$$\underset{\sim}{f} = \underset{\sim}{n}\underset{\sim}{\sigma} \tag{1.2}$$

The state of stress at a point P in a given coordinate system is uniquely determined by three stress vectors. They correspond to three base vectors of this system which

represent three planes perpendicular to each other, and intersecting at a point P. Thus, in the Cartesian coordinate system x, y, z, defined by the base vectors $\underset{\sim}{i}_x$, $\underset{\sim}{i}_y$, $\underset{\sim}{i}_z$, the stress vectors are

$$\underset{\sim}{f}\left(\underset{\sim}{i}_x\right) = \sigma_{xx}\underset{\sim}{i}_x + \sigma_{xy}\underset{\sim}{i}_y + \sigma_{xz}\underset{\sim}{i}_z \tag{1.3}$$

$$\underset{\sim}{f}\left(\underset{\sim}{i}_y\right) = \sigma_{yx}\underset{\sim}{i}_x + \sigma_{yy}\underset{\sim}{i}_y + \sigma_{yz}\underset{\sim}{i}_z \tag{1.4}$$

$$\underset{\sim}{f}\left(\underset{\sim}{i}_z\right) = \sigma_{zx}\underset{\sim}{i}_x + \sigma_{zy}\underset{\sim}{i}_y + \sigma_{zz}\underset{\sim}{i}_z \tag{1.5}$$

The stress vectors $\underset{\sim}{f}\left(\underset{\sim}{i}_x\right)$, $\underset{\sim}{f}\left(\underset{\sim}{i}_y\right)$, $\underset{\sim}{f}\left(\underset{\sim}{i}_z\right)$, respectively, act on the surfaces perpendicular to the axis of the coordinate system x, y, z (Figure 1.3).

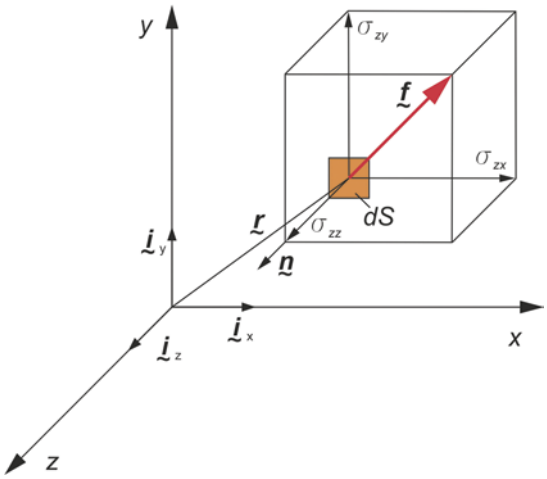

Figure 1.3
Components of the stress vector $\underset{\sim}{f}$ in the Cartesian coordinate system

As a result, the state of stress is determined by the components σ_{ij} of the corresponding stress vectors $\underset{\sim}{f}\left(\underset{\sim}{i}_x\right)$, $\underset{\sim}{f}\left(\underset{\sim}{i}_y\right)$, $\underset{\sim}{f}\left(\underset{\sim}{i}_z\right)$ and can be represented in the form of matrix:

$$\underset{\sim}{\sigma} \equiv \sigma_{ij} = \begin{vmatrix} \sigma_{xx} & \sigma_{xy} & \sigma_{xz} \\ \sigma_{yx} & \sigma_{yy} & \sigma_{yz} \\ \sigma_{zx} & \sigma_{zy} & \sigma_{zz} \end{vmatrix} \tag{1.6}$$

The first subscript i refers to the coordinate which is normal to the plane on which the stress is applied. The second subscript j defines the direction of the stress (the corresponding component of the stress vector). Thus, σ_{xy} is a shear stress acting on a plane normal to the x-axis and in the y-direction, whereas σ_{xx} is a normal stress acting on a plane normal to the x-axis and in the x-direction (Figure 1.4). It is assumed that normal stresses are positive if tensile and negative if compressive.

Table 1.3 The Equations of Momentum in Different Coordinate Systems

Cartesian system *xyz*

$$\rho\left(\frac{\partial v_x}{\partial t}+v_x\frac{\partial v_x}{\partial x}+v_y\frac{\partial v_x}{\partial y}+v_z\frac{\partial v_x}{\partial z}\right)=-\frac{\partial p}{\partial x}+\frac{\partial \tau_{xx}}{\partial x}+\frac{\partial \tau_{yx}}{\partial y}+\frac{\partial \tau_{zx}}{\partial z}+\rho g_x$$

$$\rho\left(\frac{\partial v_y}{\partial t}+v_x\frac{\partial v_y}{\partial x}+v_y\frac{\partial v_y}{\partial y}+v_z\frac{\partial v_y}{\partial z}\right)=-\frac{\partial p}{\partial y}+\frac{\partial \tau_{xy}}{\partial x}+\frac{\partial \tau_{yy}}{\partial y}+\frac{\partial \tau_{zy}}{\partial z}+\rho g_y$$

$$\rho\left(\frac{\partial v_z}{\partial t}+v_x\frac{\partial v_z}{\partial x}+v_y\frac{\partial v_z}{\partial y}+v_z\frac{\partial v_z}{\partial z}\right)=-\frac{\partial p}{\partial z}+\frac{\partial \tau_{xz}}{\partial x}+\frac{\partial \tau_{yz}}{\partial y}+\frac{\partial \tau_{zz}}{\partial z}+\rho g_z$$

Cylindrical system *rφz*

$$\rho\left(\frac{\partial v_r}{\partial t}+v_r\frac{\partial v_r}{\partial r}+\frac{v_\varphi}{r}\frac{\partial v_r}{\partial \varphi}-\frac{v_\varphi^2}{r}+v_z\frac{\partial v_r}{\partial z}\right)=-\frac{\partial p}{\partial r}+\frac{1}{r}\frac{\partial}{\partial r}\left(r\tau_{rr}\right)+\frac{1}{r}\frac{\partial \tau_{r\varphi}}{\partial \varphi}-\frac{\tau_{\varphi\varphi}}{r}+\frac{\partial \tau_{rz}}{\partial z}+\rho g_r$$

$$\rho\left(\frac{\partial v_\varphi}{\partial t}+v_r\frac{\partial v_\varphi}{\partial r}+\frac{v_\varphi}{r}\frac{\partial v_\varphi}{\partial \varphi}-\frac{v_r v_\varphi}{r}+v_z\frac{\partial v_\varphi}{\partial z}\right)=-\frac{1}{r}\frac{\partial p}{\partial \varphi}+\frac{1}{r^2}\frac{\partial}{\partial r}\left(r^2\tau_{r\varphi}\right)+\frac{1}{r}\frac{\partial \tau_{\varphi\varphi}}{\partial \varphi}+\frac{\partial \tau_{\varphi z}}{\partial z}+\rho g_\varphi$$

$$\rho\left(\frac{\partial v_z}{\partial t}+v_r\frac{\partial v_z}{\partial r}+\frac{v_\varphi}{r}\frac{\partial v_z}{\partial \varphi}+v_z\frac{\partial v_z}{\partial z}\right)=-\frac{\partial p}{\partial z}+\frac{1}{r}\frac{\partial}{\partial r}\left(r\tau_{rz}\right)+\frac{1}{r}\frac{\partial \tau_{\varphi z}}{\partial \varphi}+\frac{\partial \tau_{zz}}{\partial z}+\rho g_z$$

1.1.3.3 Conservation of Energy

The conservation of energy is based on the first law of thermodynamics. According to this law, the rate of change of total energy of a closed system is equal to the difference of the heat transferred to the system and the work done by the system to the surroundings in the unit time. The total energy is a sum of mechanical energy and thermal energy. Usually, the thermal energy is important in polymer processing.

In order to formulate the conservation law of thermal energy [37], we consider in the continuum of density $\rho(x, y, z, t)$ a control volume $\Delta x\Delta y\Delta z$ fixed in space in relation to the reference system x, y, z (Figure 1.8).

For incompressible fluids ($\rho = \text{const}$) the rate of change of energy in the control volume results from the difference in the rates of energy into and out of the control volume, and from the rate of energy dissipation (heat generation), according to the equation

$$\frac{\partial E}{\partial t}=\left(\dot{Q}_1-\dot{Q}_2\right)+\dot{W} \tag{1.67}$$

where E is the energy; t is the time; $\dot{Q}_1$ is the rate of energy into the control volume; $\dot{Q}_2$ is the rate of energy out of the control volume; $\dot{W}$ is the rate of energy dissipation in the control volume.

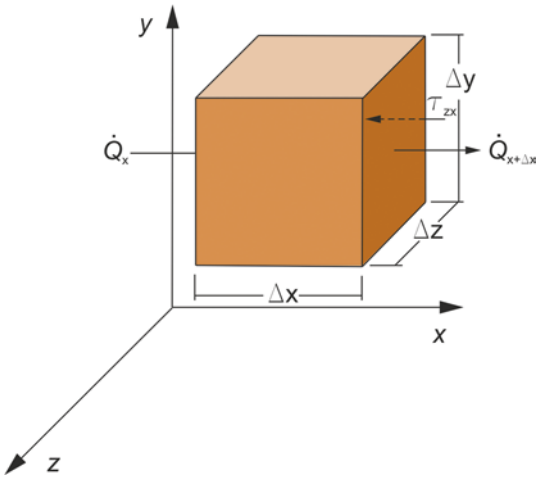

Figure 1.8
Control volume $\Delta x \Delta y \Delta z$;
the conservation law of energy

The rate of change of internal energy (energy accumulation) in the control volume is

$$\frac{\partial E}{\partial t} = \frac{\partial}{\partial t}\left(\rho e \Delta x \Delta y \Delta z\right) \tag{1.68}$$

where e is the unit internal energy of the fluid.

Since the density in the control volume is constant ($\rho = \text{const}$), Eq. (1.68) can be written as

$$\frac{\partial E}{\partial t} = \rho \frac{\partial e}{\partial t} \Delta x \Delta y \Delta z \tag{1.69}$$

The energy is transferred into the control volume or out of the control volume by heat conduction and convection. Thus

$$\dot{Q}_1 = \dot{Q}_1' + \dot{Q}_1'' \tag{1.70}$$

$$\dot{Q}_2 = \dot{Q}_2' + \dot{Q}_2'' \tag{1.71}$$

where $\dot{Q}_1'$, $\dot{Q}_2'$ are the rates of energy transferred by conduction; $\dot{Q}_1''$, $\dot{Q}_2''$ are the rates of energy transferred by convection.

Let us consider the energy transfer in the x-direction. Then, the rate of energy transferred to the control volume by conduction can be represented, using Fourier's law, as

$$\dot{Q}_x' = -k \frac{\partial T}{\partial x} \Delta y \Delta z \tag{1.72}$$

where k is the thermal conductivity; T is the temperature.

In the range of low shear rate, there is a constant ratio of shear stress to shear rate, that is, the polymer behaves like a Newtonian fluid with a constant viscosity η_0 (it is equal to the tangent of the initial slope angle α_1 of the flow curve with abscissa). Thus, the viscosity η_0 is the limit viscosity of the polymer at a shear rate tending to zero. It is referred to as the **zero shear rate viscosity:**

$$\eta_0 = \eta\left(\dot{\gamma} \to 0\right) \tag{1.108}$$

Within the range of intermediate shear rates, the ratio of shear stress to shear rate is not constant and decreases with increasing shear rate, which characterizes the behavior of non-Newtonian pseudoplastic fluids. It is characteristic that this ratio in a double logarithmic system of the shear stress versus shear rate is usually approximately constant. So, in a double-logarithmic system, the viscosity is a linear function of the shear rate. This part of the flow curve can be often well described by the power law model (Eq. (1.104)).

The second area of the Newtonian behavior of polymers occurs at very high shear rates. The slope of the flow curve is again constant, and the tangent of the slope angle α_2 determines the viscosity limit η_∞ at the shear rate tending to infinity. It is referred to as the **infinite shear rate viscosity:**

$$\eta_\infty = \eta\left(\dot{\gamma} \to \infty\right) \tag{1.109}$$

As a simplification, it can be assumed that the first area of Newtonian behavior of polymers occurs at shear rates lower than 10^{-1}–10^{1} s^{-1}. In contrast, the second Newtonian area appears at shear rates of 10^{5}–10^{6} s^{-1}. At intermediate shear rates, polymers behave like non-Newtonian pseudoplastic fluids whose flow curves can be roughly described by the power law model. It is worth adding that polymer processing is usually carried out under non-Newtonian flow conditions, i.e. at shear rates of 10^{2}–10^{4} s^{-1}.

Figure 1.15 to Figure 1.22 show examples of viscosity curves as a function of shear rate and temperature for basic thermoplastics [42], semi-crystalline polymers (LDPE, HDPE, PP, PA), and amorphous ones (PS, PVC, PMMA, PC).

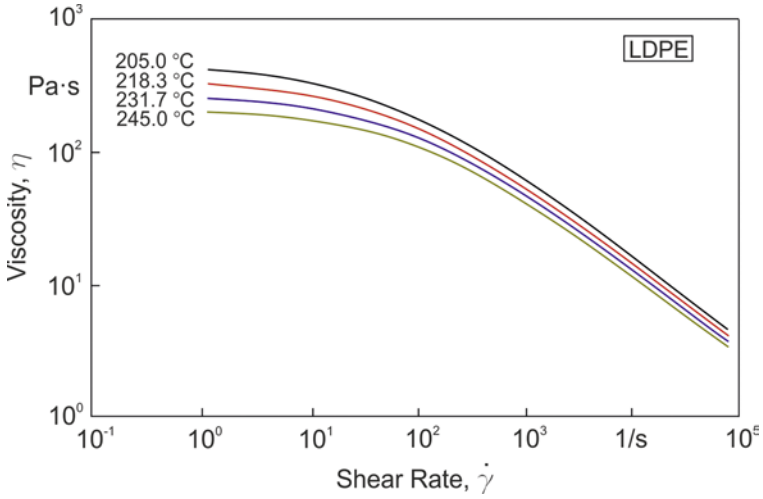

Figure 1.15 Viscosity curves of low density polyethylene (LDPE) Lupolen 1800 S (Basell Polyolefins Europe), adapted from Moldflow [42]

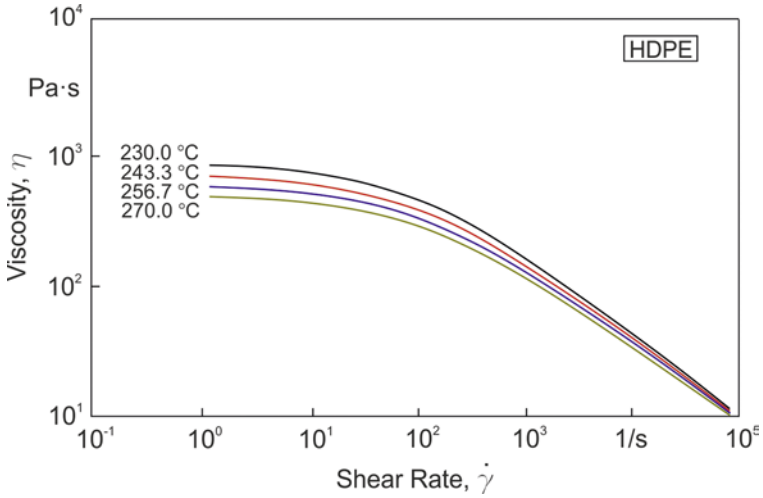

Figure 1.16 Viscosity curves of high density polyethylene (HDPE) Rigidex HD 6070 EA (BP Chemicals), adapted from Moldflow [42]

1.3.2 Characteristic Phenomena of Viscoelasticity

Viscoelastic properties of polymers are revealed and can be observed in many characteristic phenomena, e. g.

- the Weissenberg effect,
- the Barus effect,
- time effects (static and dynamic).

The **Weissenberg effect** consists in unusual formation of the free surface of a liquid in the Couette flow that is the shear flow between two coaxial cylinders, one of which rotates (Figure 1.28). During such a flow, in the case of molten polymers, the characteristic climbing of the free surface at the rotating inner cylinder is observed (Figure 1.28(a)). This phenomenon also occurs, for example, when mixing paints or varnishes. On the other hand, it does not occur in the case of Newtonian fluids, when the free surface, by neglecting the inertia force, remains flat (Figure 1.28(b)).

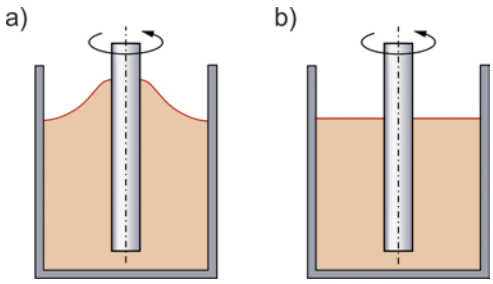

Figure 1.28
Weissenberg effect in the Couette flow:
a) molten polymer (viscoelastic),
b) Newtonian liquid

The Weissenberg effect is the result of generation of additional stresses during the shear flow, i. e. normal stresses. This is evident in Figure 1.29, which shows the shear flow between two parallel disks and, accompanying this flow, unequal formation of the liquid columns in the manometric tubes attached to one of these disks.

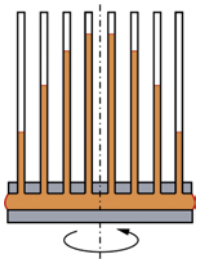

Figure 1.29
Weissenberg effect in the shear flow between two parallel disks

The **Barus effect** is an expansion of the stream of liquid flowing out of a capillary (Figure 1.30). It is often called extrudate swell or die swell, and is usually charac-

terized by the ratio of the diameter of the stream (extrudate) d to the diameter of the capillary D, that is, the so-called **degree of swelling** $B = d/D$.

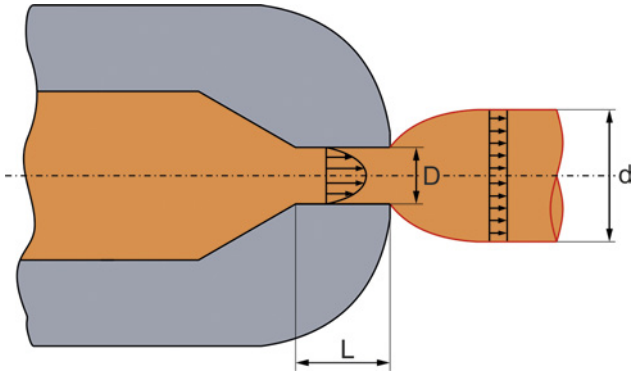

Figure 1.30 Barus effect: d – diameter of polymer stream (extrudate), D – capillary diameter, L – capillary length

Extrudate swelling is characteristic for viscoelastic materials, but also to a certain extent occurs in the case of Newtonian liquids. Then, it depends on the Reynolds number (Figure 1.31). For a Reynolds number close to zero, the Newtonian swelling is approximately 13% ($B = 1.13$). Then, it decreases with increase of the Reynolds number, and at $Re = 16$ the swelling degree is equal to unity, $B = 1.0$. In the case of Newtonian fluids, further increasing the Reynolds number results in asymptotically approaching 87% ($B = 0.87$).

In the case of polymers the extrudate swell is very large. The swelling degree is usually from 1.2 to 2.5, although sometimes it may be higher. It is characteristic that it depends largely on the flow rate of the material and the geometry of the capillary, more precisely on the ratio of the capillary length L to its diameter D (L/D).

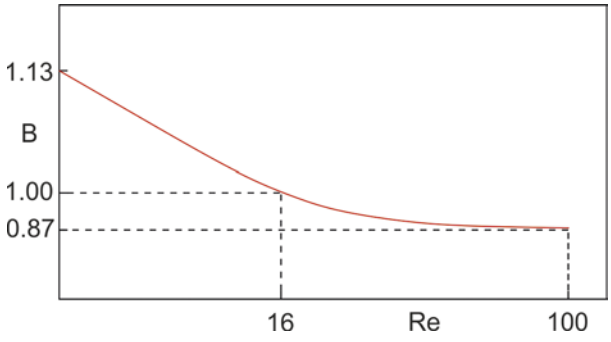

Figure 1.31 Dependence of swelling degree B on the Reynolds number Re, for the flow of Newtonian liquid through a cylindrical channel

2.2 Classification of Rheometric Methods

Rheometric methods can be divided into two groups, depending on the kinematic conditions of the measurement, i.e.

- methods implemented under shear conditions,
- methods implemented under stretching conditions.

As a result, rheometers can be divided into the shear type rheometers and the stretching type rheometers.

The shear type rheometers can be divided according to the type of flow into:

- rheometers in which shearing takes place as a result of drag flow,
- rheometers in which shearing takes place as a result of pressure flow.

The **drag flow** is the flow between two surfaces, one of which is moving and the other stationary. In contrast, the **pressure flow** is defined as the flow that takes place in a closed channel due to the pressure difference along this channel (i.e. pressure driven flow).

The basic drag flows are shown in Figure 2.1, whereas the pressure flows are depicted in Figure 2.2. Both these flows belong to the class of viscometric flows (see Section 1.3.4.2), i.e. the flows in which there is only one component of velocity, being a function of only one coordinate, not coincident with the flow direction. These flows are very important in rheometry because one can get exact (or very close to exact) solutions of the momentum equation. In addition, these flows are relatively simple in practical implementation.

According to the viscometric flows shown in Figure 2.1 and Figure 2.2, there are different types of rheometers. The most important are

- rotating rheometers
  - with coaxial cylinders (Figure 2.1(b)),
  - cone-and-plate rheometers (Figure 2.1(c)),
  - plate-and-plate rheometers (Figure 2.1(d)),
- pressure rheometers
  - capillary rheometers (Figure 2.2(a)),
  - slit rheometers (Figure 2.2(b)).

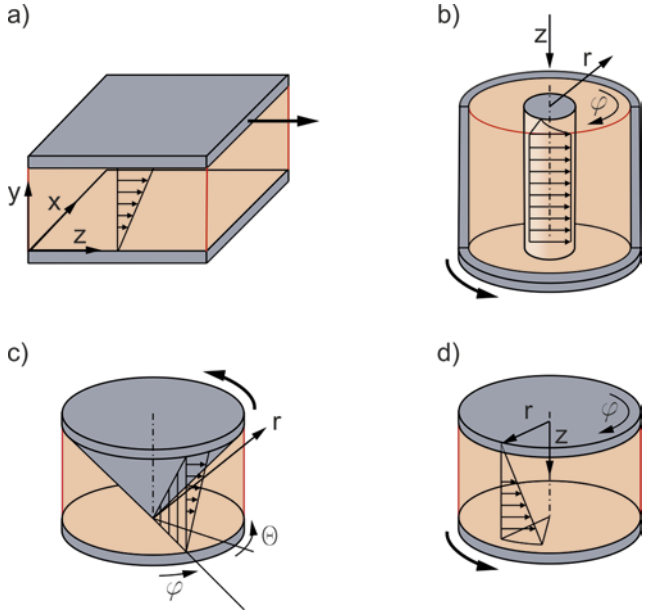

Figure 2.1 Drag flows: a) the flow between parallel (sliding) plates, b) the flow between coaxial cylinders (Couette flow), c) the flow between cone and plate, d) the flow between two plates (torsional flow)

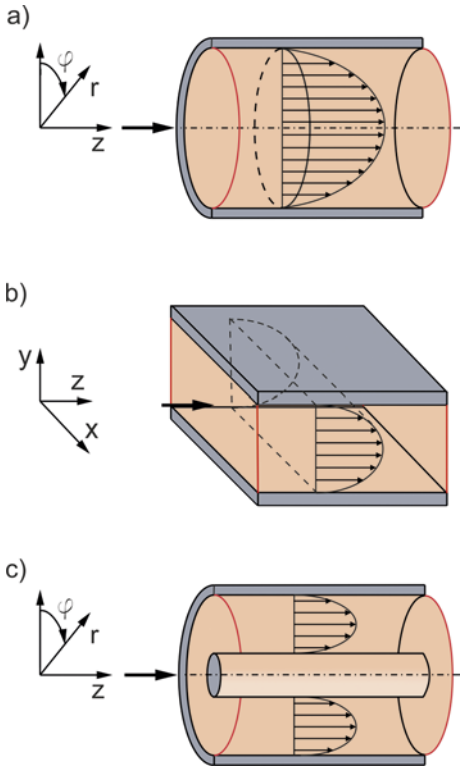

Figure 2.2
Pressure flows: a) the flow in a cylindrical channel (Poiseuille flow), b) the flow in a slit channel (between two parallel plates), c) the flow in an annular channel

2.5.2 Theoretical Basics

General Assumptions

The schematic of the cone-plate rheometer is shown in the spherical coordinate system r, θ, φ in Figure 2.22. The basic assumptions of the flow are as follows:

- the flow is steady, laminar, and isothermal,
- there is no slip on the cone and plate,
- gravity and inertia forces are neglected,
- the fluid is incompressible and its viscosity does not depend on the pressure,
- $\alpha < 0.05$ rad ($\approx 3°$),
- the velocity field has the form

$$v_r = 0, \quad v_\theta = 0, \quad v_\varphi = v_\varphi(r,\theta) \tag{2.78}$$

- shearing occurs on conical surfaces $\theta\varphi$ of the same apex as the cone of the measuring system, rotating at an angular velocity $\omega = \omega(\theta)$ around the axis of this system, such that

$$v_\varphi = r\omega(\theta)\sin\theta \tag{2.79}$$

where, on the basis of the non-slip condition

$$v_\varphi(\pi/2) = 0 \tag{2.80}$$

$$v_\varphi(\pi/2-\alpha) = \Omega r \sin(\pi/2-\alpha) \tag{2.81}$$

where Ω is the angular velocity (the frequency) of the cone.

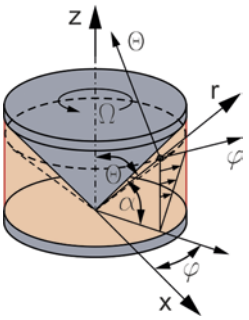

Figure 2.22
Cone-and-plate rheometer: φ – flow direction, θ – direction of velocity change, r – neutral direction

Under assumed flow conditions, the shear rate $\dot{\gamma}$ is expressed as the component $2D_{\theta\varphi}$ of the strain rate tensor $2\underset{\sim}{\boldsymbol{D}}$. In the general case, this component is equal to [16]

$$D_{\theta\varphi} = \frac{1}{2}\left[\frac{\sin\theta}{r}\frac{\partial}{\partial\theta}\left(\frac{v_\varphi}{\sin\theta}\right) + \frac{1}{r\sin\theta}\frac{\partial v_\theta}{\partial\varphi}\right] \tag{2.82}$$

Taking into account that $v_\theta = 0$ (Eq. (2.78)) and applying Eq. (2.79), the shear rate is determined by

$$\dot{\gamma} = 2D_{\theta\varphi} = \frac{\mathrm{d}\omega}{\mathrm{d}\theta}\sin\theta \tag{2.83}$$

Assuming that the angle α is very small, the shear rate may be approximately expressed by

$$\dot{\gamma} \approx \frac{\Omega}{\alpha}\sin(\pi/2) \approx \frac{\Omega}{\alpha} \tag{2.84}$$

It is therefore independent of the coordinate θ.

The constant shear rate in the gap means that the shear stress should also be constant. Determination of this stress will make it possible to determine the viscosity for this shear rate.

Determination of Viscosity

In order to determine the shear stress, the equation of motion in the direction of coordinate φ can be considered [20]. Under assumed flow conditions, this equation is expressed by

$$0 = \frac{1}{r}\frac{\partial\tau_{\theta\varphi}}{\partial\theta} + \frac{2}{r}\tau_{\theta\varphi}\cot\theta \tag{2.85}$$

and, after replacing partial derivatives with ordinary derivatives and simplification, it takes the form

$$\frac{\mathrm{d}\tau_{\theta\varphi}}{\mathrm{d}\theta} = -2\tau_{\theta\varphi}\cot\theta \tag{2.86}$$

Integrating this expression leads to

$$\tau_{\theta\varphi} = \frac{C}{\sin^2\theta} \tag{2.87}$$

where the constant C is equal to the stress $\tau_{\theta\varphi}|_{\pi/2}$ on the plate surface, since $\tau_{\theta\varphi}(\theta = \pi/2) = \tau_{\theta\varphi}|_{\pi/2}$.

The stress $\tau_{\theta\varphi}|_{\pi/2}$ can be determined from the torque balance on the surface of the plate of radius R. This balance is made by integrating relative to this surface the product of stress $\tau_{\theta\varphi}|_{\pi/2}$ and infinitesimal surface of the plate $r\mathrm{d}r\mathrm{d}\varphi$ and radius r, so that this torque expresses as

4.2.1.3 Flow through a Tapered Channel

The schematic of flow in a tapered slit is depicted in the Cartesian system *xyz* in Figure 4.6.

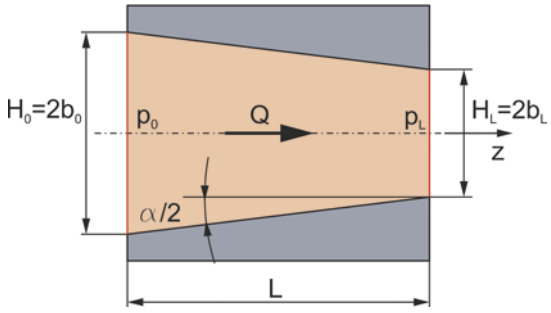

Figure 4.6 Schematic of flow in a tapered slit: Q – volume flow rate, p_0 – pressure at channel inlet, p_L – pressure at channel outlet

The flow will be considered as isothermal and Newtonian. Furthermore, assuming that the angle of convergence $2\alpha < 30°$, it is reasonable to consider this flow as being close to the flow between parallel plates [30].

Based on this assumption, Eq. (4.18) obtained for the flow between parallel plates (see Section 4.2.1.1 – Isothermal Newtonian Flow) is applied. For this case, it will be convenient to write it in the form

$$\Delta p = \frac{3L}{2Wb^3}\mu Q \tag{4.126}$$

where $b = H/2$.

On the basis of Eq. (4.4), Eq. (4.126) can be presented with reference to the infinitesimal length dz as

$$\mathrm{d}p = -\frac{3\mu Q}{2Wb^3}\mathrm{d}z \tag{4.127}$$

where dp is the pressure drop along the length dz.

Dimension b is a function of the location in the z-axis direction and expresses as

$$b = b_0 - \frac{b_0 - b_L}{L}z \tag{4.128}$$

where $b_0 = H_0/2$ and $b_L = H_L/2$ are the dimensions at the inlet and outlet of the channel.

On the basis of Eq. (4.128), the length dz can be determined as

$$\mathrm{d}z = -\frac{L}{b_0 - b_L}\mathrm{d}b \tag{4.129}$$

and Eq. (4.127) can be transformed to

$$\mathrm{d}p = \frac{3\mu Q}{2W}\frac{L}{b_0 - b_L} b^{-3}\mathrm{d}b \tag{4.130}$$

After integrating Eq. (4.130) as follows

$$\int_{p_0}^{p_L} \mathrm{d}p = \frac{3\mu Q}{2W}\frac{L}{b_0 - b_L}\int_{b_0}^{b_L} b^{-3}\mathrm{d}b \tag{4.131}$$

we get

$$p_L - p_0 = -\frac{3\mu Q}{2W}\frac{L}{b_0 - b_L}\frac{1}{2}\left(\frac{1}{b_L^2} - \frac{1}{b_0^2}\right) \tag{4.132}$$

and finally

$$\Delta p = p_0 - p_L = \frac{3\mu QL}{4W}\frac{b_0 + b_L}{b_0^2 b_L^2} \tag{4.133}$$

or

$$\Delta p = \frac{6L}{W}\frac{H_0 + H_L}{H_0^2 H_L^2}\mu Q \tag{4.134}$$

It is easy to check that for $b_0 = b_L = b$ or $H_0 = H_L = H$, i. e. for the parallel channel, this formula reduces to Eq. (4.18) or Eq. (4.126).

4.2.1.4 Flow through a Cone

The schematic of flow in a truncated cone in the cylindrical system $r\varphi z$ is depicted in Figure 4.7.

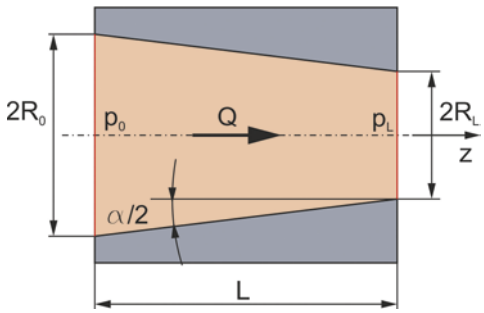

Figure 4.7 Schematic of flow in a truncated cone: Q – volume flow rate, p_0 – pressure at channel inlet, p_L – pressure at channel outlet

The flow will be considered as isothermal and Newtonian. Furthermore, assuming that the angle of convergence $2\alpha < 30°$, it is reasonable to consider this flow as being close to the flow in a tube [30].

The flow rate in the working space is equal to

$$Q_o = \frac{Q}{i_o} \tag{5.153}$$

and the equivalent radius can be expressed as

$$R_h = \left(\frac{A}{\pi}\right)^{1/2} \tag{5.154}$$

where Q is the total flow rate; i_o is the number of working spaces in the ring; A is the cross-section of working space.

5.2.7 Characteristics of Extruder Operation

The extrusion process is the result of cooperation between the screw and the die.

The equation of the polymer flow rate in the extruder, in reference to the Newtonian model, is expressed by Eq. (5.93). This equation, after taking into account the leakage flow (Eq. (5.108)) and the effect of the flight flanks on the flow rate (Eq. (5.103)), and after replacing the pressure gradient along the length of the screw channel with the gradient along the screw axis, can be presented as

$$Q = \frac{\pi D_b N \cos\varphi_b WH}{2}\left(1-\frac{h_f}{H}\right)F_d - \frac{WH^3}{12\eta}\frac{\Delta p}{L}\sin\varphi_a\left(1+f_1\right)F_p \tag{5.155}$$

or in the form

$$Q = \alpha N - \beta\frac{\Delta p}{\eta} \tag{5.156}$$

where α, β are the geometrical constants defined as

$$\alpha = \frac{\pi D_b N \cos\varphi_b WH}{2}\left(1-\frac{h_f}{H}\right)F_d \tag{5.157}$$

$$\beta = \frac{WH^3}{12L}\sin\varphi_a\left(1+f_1\right)F_p \tag{5.158}$$

where N is the screw rotational speed; Δp is the pressure change in the metering zone, the difference between the pressure at the end of the screw and the pressure at the beginning of the metering zone, i.e. $\Delta p = p_L - p_0$; L is the length of the metering zone; φ_b, φ_a is the helix angle, on the barrel surface and halfway up the channel, respectively.

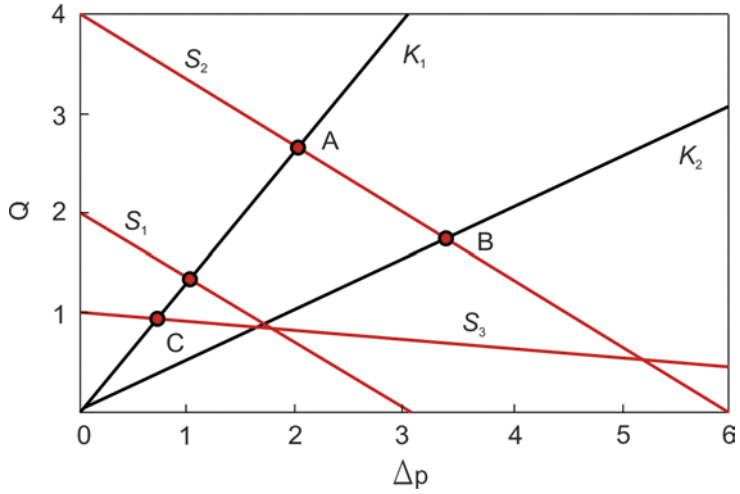

Figure 5.27 Extruder operating characteristics (Newtonian flow): Q – volume flow rate; Δp – pressure change in the extruder (increase) and in the die (drop); $S_1(H, N)$, $S_2(H, 2N)$, $S_3(H/2, N)$ – screw characteristics; H – screw channel depth; N – screw rotational screw; K_1, K_2 die characteristics, K – die conductivity, $K_1 > K_2$; A, B, C – extruder operating points

The flow rate equation for the screw (Eq. (5.156)), in the coordinate system of volume flow rate and pressure change, is represented by a straight line with a negative angle coefficient, which is the **screw characteristics** (Figure 5.27).

The flow rate equation for the die, with reference to the Newtonian model, can be expressed as

$$Q = K\frac{\Delta p}{\eta} \tag{5.159}$$

where Δp is the pressure drop in the die; K is the geometrical constant (conductivity).

This equation, in the coordinate system of volume flow rate and pressure change, is represented by a straight line with a positive angle coefficient, which is the **die characteristics** (Figure 5.27).

The extruder, from the point of view of flow conditions, is a serial connection of the barrel (screw) and the die, so that the formulas in Eq. (5.165) apply here.

For the sake of simplicity, a further analysis of the screw/die interactions are made with respect to the melt extrusion, i. e. assuming that the material is fed into the extruder as a melt.

Because, omitting the hopper, the pressure at the extruder inlet and the pressure at the die outlet are equal to atmospheric pressure, the pressure increase in the screw Δp_{screw} will be equal to the pressure drop in the die Δp_{die}, i. e.

$$\Delta p_{screw} = \Delta p_{die} \tag{5.160}$$

6 Computer Modeling for Polymer Processing

6.1 Overview of Computer Modeling Software

Software for computer modeling of polymer processing can be divided into two groups: **generally oriented systems** (i. e. general purpose) and **systems oriented on a specific processing technique** (e. g. extrusion or injection molding). The operation of these systems is based on solving equations of continuum mechanics (mass, momentum, and energy) for specific material models under specific flow conditions.

In the group of generally oriented systems, i. e. CFD systems (Computational Fluid Dynamics), several program packages can be distinguished, e. g.:

- ANSYS Polyflow (ANSYS, Inc., Canonsburg, PA, USA),
- ANSYS Fluent (ANSYS, Inc., Canonsburg, PA, USA),
- Autodesk CFD (Autodesk, Inc., San Rafael, CA, USA),
- OpenFOAM (The OpenFOAM Foundation, Ltd., London, UK),
- FLOW-3D (Flow Science, Inc., Pasadena, CA, USA),
- COMSOL Multiphysics (COMSO, Inc., Burlington, MA, USA).

The second group of modeling systems concerns clearly formulated issues and is limited to a specific type of processing techniques, e. g. extrusion and injection molding.

In the group of systems for simulation of injection molding (more precisely for simulation of flow in injection molds), the following program packages can be distinguished:

- Autodesk Moldflow (Autodesk, Inc., San Rafael, CA, USA),
- Moldex3D (CoreTech System Co., Ltd., Chupei City, Hsinchu County, Taiwan),
- CADMOULD 3D-F (Simcon GmbH, Wuerselen, Germany),
- SIGMASOFT Virtual Molding (SIGMA Engineering GmbH, Aachen, Germany),

- SIMULIA (Dassault Systemes, Vélizy-Villacoublay, France),
- REM 3D (TRANSFALOR S. A., Sophia Antipolis, France).

It is important to note that the only available software for simulation of flow in the injection molding machine is

- PSI (Paderborn University, Paderborn, Germany).

In the group of systems for simulation of extrusion, the following program packages for simulation of single screw extrusion can be distinguished:

- EXTRUD (Scientific Process & Research, Inc., Somerset, NJ, USA) – historically the first,
- NEXTRUCAD (Polydynamics, Inc., Dundas, Ontario, Canada),
- REX (Paderborn University, Paderborn, Germany),
- COMPUPLAST (Compuplast International Inc., Zlin, Czech Republic),
- WIN SSD (Stevens Institute of Technology, Hoboken, NJ, USA),
- CEMEXTRUD (CEMEF – Centre for Materials Processing, Ecole des Mines, Sophia Antipolis, France),
- GSEM (Warsaw University of Technology, Warsaw, Poland).

In the case of twin screw extrusion, the following program packages for simulation of co-rotating extrusion can be distinguished:

- AKRO-CO-TWIN SCREW (The University of Akron, Akron, OH, USA) – historically the first,
- SIGMA (Paderborn University, Paderborn, Germany),
- Ludovic (Sciences Computers Consultants, Inc., Saint-Etienne, France),
- WinTXS (PolyTech, New Haven, CT, USA).

as well as for simulation of counter-rotating extrusion:

- AKRO-COUNTER-TWIN SCREW (University of Akron, Akron, OH, USA) – historically the first,
- TSEM (Warsaw University of Technology, Warsaw, Poland).

Modeling with generally oriented systems is different from modeling with specific oriented systems. The basis of the first type of modeling is to define the considered problem each time, while in the second case the problem to be solved is already defined. Apart from this difference, modeling using various systems is similar. In any case, it consists in entering into the program data on the flow geometry, flow conditions, and material characteristics, and then performing computations.

The basic flow problems in polymer processing can be solved using CFD software, and the software for modeling of injection molding and extrusion. The selected flow problems presented in the further part of this chapter were solved using

- selecting the injection molding machine,
- setting the velocity/pressure switch-over point from the ram speed control to the packing pressure control which typically takes place before the cavity is filled,
- process settings, e. g. the Filling Control Profile setting which is used to enter filling profiles to vary the ram movement during the filling phase, the Pack Control Profile setting which is used to enter packing profiles to vary the pressure applied to the cavity during the packing phase, and the Mold Surface Temperature Profile setting which is used to enter the mold surface temperature profile of zones of the mold through the injection molding cycle,
- optimization analyses,
- checking the simulation results.

6.3.3 Examples of Modeling

Autodesk Moldflow can be used to simulate various injection molding processes to solve various flow problems and perform various process analyses. In the further part of this section, the examples of important analyses are presented, i. e. the gate location, the filling analysis, and the flow balancing. Some details of these analyses are presented in the literature [36–39].

6.3.3.1 Gate Location

The Gate Location analysis is used to recommend injection locations for the part. This analysis works for all analysis technologies and is used as a preliminary input for a full Fill & Pack analysis. A Runner Balance analysis can be used with a Fill analysis to ensure equal pressure is delivered at each cavity.

After running a Gate Location analysis, the recommended injection location is automatically displayed, as depicted in Figure 6.62 on an example of a tensile test specimen.

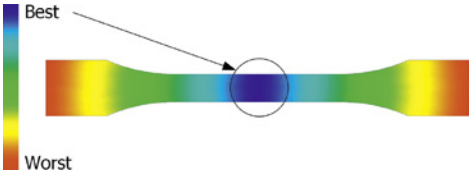

Figure 6.62
Gate Location analysis

6.3.3.2 Filling Analysis

The Fill analysis predicts the thermoplastic polymer flow inside the mold in the filling phase. This analysis is often run as the first part of a Fill & Pack analysis sequence. In this section, the Fill analysis is presented on an example of the double-cavity mold for tensile test specimens with two different gate locations with edge and lateral gating. It is performed for polypropylene.

This analysis calculates the flow front that grows through the part incrementally from the injection location, and continues until the velocity/pressure switch-over point has been reached. This is depicted in Figure 6.63.

Moreover, the filling analysis allows us to simulate the distribution of various flow parameters, e. g. velocity, pressure, temperature, etc., which are depicted in Figure 6.64 to Figure 6.66. It is seen that various gate locations result in various distributions of these parameters, and finally in various part deflections, which are shown in Figure 6.67.

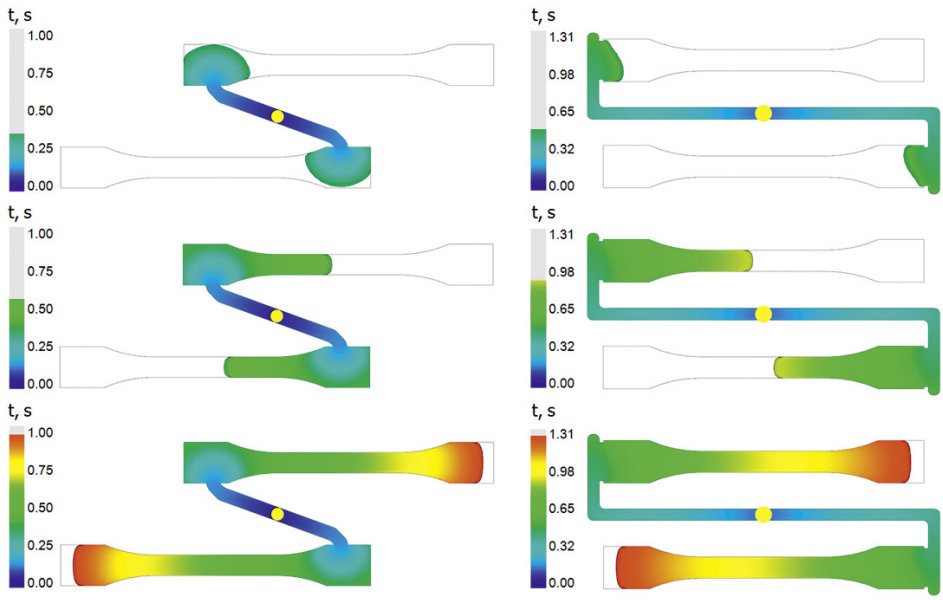

Figure 6.63 Fill analysis – edge vs lateral gating: growth of the flow front

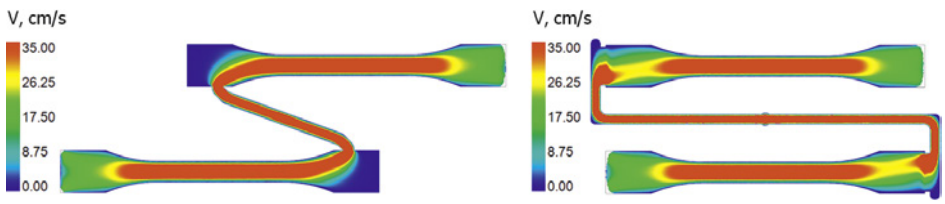

Figure 6.64 Fill analysis – edge vs lateral gating: velocity distribution

Index

E

F

G

P

R

S

T

V

W

Z